Molecular mechanisms of Evening Complex activity in *Arabidopsis*

Catarina S. Silva[a,1,2,3], Aditya Nayak[a,1,4], Xuelei Lai[a,1], Stephanie Hutin[a,3], Véronique Hugouvieux[a], Jae-Hoon Jung[b], Irene López-Vidriero[c], Jose M. Franco-Zorrilla[c], Kishore C. S. Panigrahi[d], Max H. Nanao[e], Philip A. Wigge[f], and Chloe Zubieta[a,3]

[a]Laboratoire de Physiologie Cellulaire and Végétale, Université Grenoble Alpes/Centre National de la Recherche Scientifique/Commissariat à l'Énergie Atomique et aux Énergies Alternatives/Institut National de la Recherche Agronomique/Interdisciplinary Research Institute of Grenoble, 38054 Grenoble, France; [b]Department of Biological Sciences, Sungkyunkwan University, 16419 Suwon, Korea; [c]Genomics Unit, Centro Nacional de Biotecnología–Consejo Superior de Investigaciones Científicas, 28049 Madrid, Spain; [d]Plant Biology Laboratory, School of Biological Sciences, National Institute of Science Education and Research, Bhubaneshwar, India 752050; [e]Structural Biology Group, European Synchrotron Radiation Facility, 38043 Grenoble, France; and [f]Department for Plant Adaptation, Leibniz-Institut für Gemüse- und Zierpflanzenbau, 14979 Grossbeeren, Germany

Edited by George Coupland, Max Planck Institute for Plant Breeding Research, Cologne, Germany, and approved February 13, 2020 (received for review December 3, 2019)

The Evening Complex (EC), composed of the DNA binding protein LUX ARRHYTHMO (LUX) and two additional proteins EARLY FLOWERING 3 (ELF3) and ELF4, is a transcriptional repressor complex and a core component of the plant circadian clock. In addition to maintaining oscillations in clock gene expression, the EC also participates in temperature and light entrainment, acting as an important environmental sensor and conveying this information to growth and developmental pathways. However, the molecular basis for EC DNA binding specificity and temperature-dependent activity were not known. Here, we solved the structure of the DNA binding domain of LUX in complex with DNA. Residues critical for high-affinity binding and direct base readout were determined and tested via site-directed mutagenesis in vitro and in vivo. Using extensive in vitro DNA binding assays of LUX alone and in complex with ELF3 and ELF4, we demonstrate that, while LUX alone binds DNA with high affinity, the LUX–ELF3 complex is a relatively poor binder of DNA. ELF4 restores binding to the complex. In vitro, the full EC is able to act as a direct thermosensor, with stronger DNA binding at 4 °C and weaker binding at 27 °C. In addition, an excess of ELF4 is able to restore EC binding even at 27 °C. Taken together, these data suggest that ELF4 is a key modulator of thermosensitive EC activity.

circadian clock | gene regulation | Evening Complex | protein–DNA complex

The circadian clock provides endogenous rhythms that allow plants to anticipate and react to daily environmental changes. Many processes, such as photosynthesis and growth, occur in a rhythmic manner over a 24-h cycle (1–3). These circadian rhythms persist even in the absence of light/dark cues due to internal repeating oscillations of core clock genes that in turn modulate gene expression patterns of many different output pathways (4). In *Arabidopsis*, the circadian clock consists of three main interacting transcription–translation feedback loops: the morning, central, and evening loops. Components of these interlocking feedback loops repress each other's expression, resulting in rhythmic gene expression over a 24-h period (reviewed in refs. 3 and 5–7). The Evening Complex (EC), composed of LUX ARRHYTHMO (LUX), EARLY FLOWERING 3 (ELF3), and ELF4, is a core component of the circadian clock (8–12). The expression patterns of the three genes overlap and peak at dusk. Thus, the EC has maximum activity at the end of the day and early night, acting to repress expression of the circadian morning loop genes *PSEUDORESPONSE REGULATOR 7* (*PRR7*) and *PRR9*, the central loop gene *CCA1*, and the evening loop genes *GIGANTEA* (*GI*) and *LUX* itself (12–15).

Loss-of-function mutations in *elf3, elf4*, or *lux* give rise to arrhythmic circadian outputs with alterations in many developmental pathways (9, 16–18). Derepression of key regulators of thermomorphogenesis, such as the basic helix–loop–helix (bHLH) transcription factor (TF) *PHYTOCHROME INTERACTING FACTOR 4* (*PIF4*), results in phenotypes including elongated hypocotyls and early flowering (9, 12, 16–19). Natural variation in EC components *ELF3* and *LUX* has been shown to give rise to altered thermal responsive growth not only in *Arabidopsis* but also in crop plants (20–23). Thus, activation of thermomorphogenesis even at low temperatures and early flowering in EC mutants are due in large part to misregulation of the circadian output pathway involving *PIF4*, a master regulator of cell elongation, thermoresponsive growth, and the shade avoidance response (19, 24–28).

The repressive regulatory activity of the EC is temperature dependent, making it a node that integrates both circadian gene regulation and environmental information to control growth and

Significance

Circadian gene expression oscillates over a 24-h period and regulates many genes critical for growth and development in plants. A key component of the circadian clock is the Evening Complex (EC), a transcriptional repressor complex that contains the proteins LUX ARRHYTHMO, EARLY FLOWERING 3, and EARLY FLOWERING 4 (ELF4). By repressing the expression of genes such as *PHYTOCHROME INTERACTING FACTOR4* (*PIF4*), the EC reduces elongation growth. At warmer temperatures, EC activity is lost, promoting thermomorphogenesis via *PIF4* expression. The molecular mechanisms underlying EC activity are not well understood. Here, we combined structural studies with extensive in vitro assays to determine the molecular mechanisms of the temperature-dependent EC binding to DNA and demonstrate the critical role of ELF4 in this activity.

Author contributions: C.S.S., X.L., S.H., K.C.S.P., P.A.W., and C.Z. designed research; C.S.S., A.N., X.L., S.H., V.H., J.-H.J., I.L.-V., J.M.F.-Z., and M.H.N. performed research; C.S.S., A.N., S.H., J.M.F.-Z., M.H.N., P.A.W., and C.Z. analyzed data; and C.Z. wrote the paper with contributions from the authors.

The authors declare no competing interest.

This article is a PNAS Direct Submission.

This open access article is distributed under Creative Commons Attribution-NonCommercial-NoDerivatives License 4.0 (CC BY-NC-ND).

Data deposition: The crystallography, atomic coordinates, and structure factors reported in this paper have been deposited in the Protein Data Bank (ID codes 5LXU and 6QEC).

[1]C.S.S., A.N., and X.L. contributed equally to this work.

[2]Present address: European Molecular Biology Laboratory, 38042 Grenoble, France.

[3]To whom correspondence may be addressed. Email: Csilva@embl.fr, stephanie.hutin@univ-grenoble-alpes.fr, or Chloe.Zubieta@cea.fr.

[4]Present address: Institute of Molecular Plant Biology, Department of Biology, ETH Zürich, 8092 Zürich, Switzerland.

This article contains supporting information online at https://www.pnas.org/lookup/suppl/doi:10.1073/pnas.1920972117/-/DCSupplemental.

First published March 12, 2020.

Downloaded at Palestinian Territory, occupied on December 27, 2021

www.manaraa.com

developmental pathways in plants (14, 20, 29). Extensive chromatin immunoprecipitation sequencing (ChIP-seq) experiments performed at different temperatures demonstrated that the binding sites for LUX, ELF4, and ELF3 extensively overlap and that the interaction strength is dependent on temperature, with weaker binding of the complex at higher temperatures, suggesting that the EC may act as a direct thermosensor (15). The underlying mechanisms that determine EC complex formation and DNA binding, however, remained to be elucidated. Here, we address the molecular determinants of DNA binding affinity and specificity by structurally characterizing the DNA binding domain (DBD) of LUX in complex with DNA. Furthermore, we determine the role of each protein in EC formation using in vitro assays and demonstrate a role for ELF4 in stabilizing EC binding to DNA.

Results

LUX and the LUX MYB Domain Bind DNA with High Affinity Independently of the EC. LUX possesses a single MYB DBD, whereas ELF3 and ELF4 have no domains known to interact with DNA. In order to determine whether LUX alone was sufficient to confer DNA binding affinity and specificity, we analyzed the DNA binding activity of the full-length (FL) protein (LUX^{FL}) and the DNA binding MYB domain (residues 139 to 200, LUX^{MYB}) using protein binding microarrays (PBMs). In both cases, the proteins were tagged with an N-terminal maltose binding protein (MBP). Experiments were performed and analyzed as previously described (30, 31). LUX^{FL} yielded over 100 high-affinity binding 8-mers with E scores over 0.45, indicative of high-affinity binding. Most motifs correspond to variations of the sequence "AGAT(A/T)CG" as previously determined in vivo (10) (Fig. 1*A*). The isolated DBD LUX^{MYB} bound with lower affinity, producing consensus motifs with the majority of E scores below 0.35, with only two 8-mers identified with E scores above 0.45 (*SI Appendix*, Fig. S1).

As LUX has only a single MYB domain, the absolute binding affinities of untagged LUX^{FL} and LUX^{MYB} were assayed to determine whether this single domain is sufficient to target the EC to its cognate binding sites. To confirm the affinity of LUX–DNA interactions, DNA sequences with variations of the LUX binding site (LBS) were tested against varying protein concentrations using electrophoretic mobility shift assays (EMSAs). Surprisingly, LUX^{MYB} exhibited higher affinity compared with the full-length protein for all DNA probes tested, with K_d values ranging from 6.5 to 43 nM (Fig. 1*B* and Table 1), in comparison with the full-length protein that exhibited lower affinity over the sequences tested, with K_d values in the 90- to 180-nM range (Fig. 1*C* and Table 1). All K_d measurements were performed on untagged proteins, unlike the PBM experiments. The PBM result indicating a lower affinity of LUX^{MYB} for DNA is thus likely due to the N-terminal MBP fusion, which may occlude the DNA binding site and suggests that large protein fusions close to the N terminus of the MYB domain negatively impact DNA binding. As the LUX DBD is embedded within the full-length protein with both N- and C-terminal unstructured regions adjacent to the DBD, the DNA binding affinity is likely affected by the accessibility of the DBD.

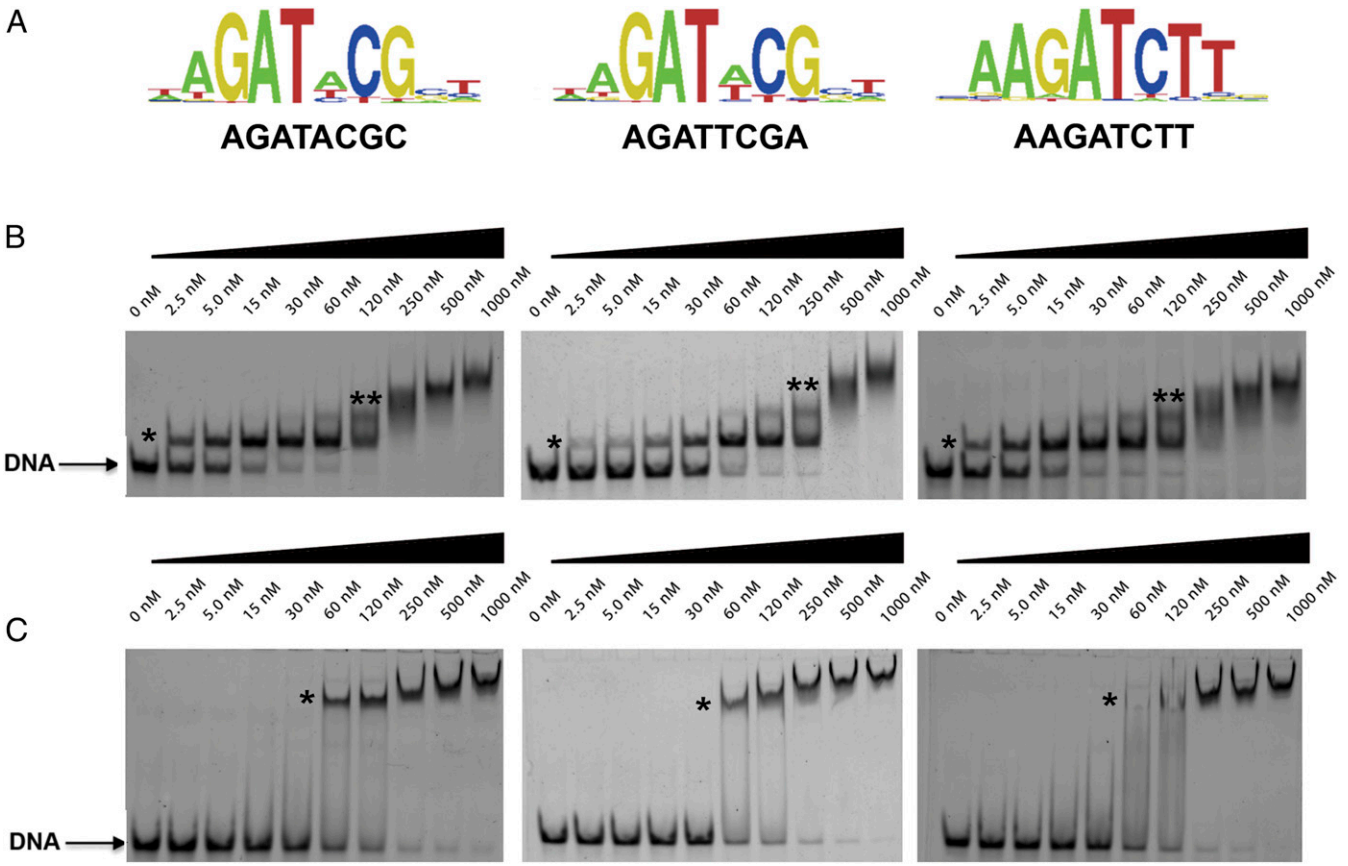

Fig. 1. LUX–DNA interactions. (*A*) High-scoring PBM-derived logos for LUX. Three logos are presented, including the LBS consensus (*Left*), the *PRR9* promoter LBS sequence (*Center*), and a high-scoring PBM sequence (*Right*). (*B*) Representative gel EMSAs for LUX^{MYB}. DNA concentration was constant with protein concentration increasing from 0 to 1,000 nM. The DNA sequences used correspond to the above motifs in *A*. Free DNA is indicated by an arrow, and protein–DNA complexes are indicated with stars. One star corresponds to one molecule of protein bound; two stars indicates multiple nonspecifically bound protein molecules at high protein concentrations. (*C*) Representative EMSA for LUX^{FL} labeled as per *B*.

Downloaded at Palestinian Territory, occupied on December 27, 2021

www.manaraa.com

Table 1. DNA binding affinities of LUX^{MYB} and LUX^{FL} and respective mutants

LBS 8-mer motifs	LUX^{MYB} (nM)	LUX^{FL} (nM)	LUX^{MYB} R146A (nM)	LUX^{FL} R146A (nM)
AGATTCGA (*PRR9*)	37 ± 2.9	93 ± 5.8	50 ± 2.4	105 ± 11.8
AGATACGC (crystal)	6.5 ± 1.4	98 ± 2.9	50 ± 1.8	336 ± 4.8
AAGATCTT	14 ± 1.8	93 ± 3.5	63 ± 3.1	204 ± 6.7
GGATCCGA	17 ± 2.1	118 ± 10.6	120 ± 1.0	164 ± 4.2
ATATTCGA (crystal)	43 ± 4.2	178 ± 3.5	137 ± 13.0	nd

Not determined (nd), binding was too weak to measure.

Potential additional amino acid contributions present in the full-length protein may also tune the specificity of the DBD as the PBM motifs varied for the full-length and DBD constructs. Overall, these data demonstrate that LUX is able to bind with high affinity to its cognate sites in the low-nanomolar range and that this high-affinity binding is likely sufficient to target the entire EC to these sites genome wide.

The GARP Family Signature Motif in LUX Is Required for Base Readout. Having determined the in vitro binding specificity and affinity of LUX^{FL} and LUX^{MYB} with DNA, we sought to reveal the molecular determinants for DNA binding specificity. We crystallized LUX^{MYB} in complex with a 10-mer double stranded DNA (dsDNA), 5′-TAGATACGCA-3′ and 5′-ATGCGTATCT-3′ (complementary strand), with a one-base overhang containing the core binding motif (underlined) determined from the PBM experiments and LUX^{MYB} in complex with a second DNA sequence with a one-base overhang, 5′-TATATTCGAA-3′ and 5′-ATTCGAATAT-3′ (complementary strand), which lacks the highly conserved guanine at the beginning of the LBS and replaces the adenine with a thymine, a conservative change in the LBS consensus sequence GAT(A/T)CG (Table 2). For both structures, LUX^{MYB} adopts a classic three-helix bundle conformation characteristic of MYB domains (Fig. 2). The MYB hydrophobic core usually consists of three regularly spaced residues, most often tryptophans, with a spacing of 18 or 19 amino acids (*SI Appendix*, Fig. S2) (32). In LUX^{MYB}, however, the second and third tryptophan residues are replaced by a proline (Pro171) and a leucine (Leu192) based on structural alignments. Proline at position 171 creates a tight turn before helix 2 and brings the helix in close proximity to the DNA. A proline at this position is also conserved in other plant MYB proteins, such as the structurally characterized transcription factor, AtARR10 (*SI Appendix*, Fig. S2). Interestingly, in a strong *lux* mutant allele, Pro171 is replaced by a leucine residue, suggesting that the tight turn before helix 2 is required for proper interaction of the protein with DNA. We confirmed this hypothesis by comparing DNA binding of LUX with LUX^{P171L} (*SI Appendix*, Fig. S3). In EMSAs, we observed no DNA shift for LUX with the proline to leucine mutation, suggesting that indeed DNA binding is abrogated due to this mutation. The hydrophobic core in LUX^{MYB} is further stabilized by additional hydrophobic interactions, including edge-to-face interactions of Phe157 (helix 1) and Tyr195 (helix 3), π stacking of Trp149 (helix 1) with His191 (helix 3), and edge-to-face interactions of His191 and Phe157 (Fig. 2*A*). The protein sequesters DNA primarily through helix 3 that lies in the major groove and contains a plant-specific GARP family (named for GOLDEN2 from aize, ARR B-class from *Arabidopsis* and Psr1 from *Chlamydomonas*) signature motif, SH(A/L)QK(F/Y) (16). Examination of the electrostatic surface of the protein demonstrates a highly electropositive face that acts as the main DNA binding surface (Fig. 2*B*).

Table 2. Data collection and refinement statistics

	LUX^{MYB} 5′-TAGATACGCA	LUX^{MYB} 5′-TATATTCGAA
Data collection		
Space group	$P2_1$	$P2_1$
Cell dimensions		
a, *b*, *c* (Å)	42.16, 32.83, 53.76	32.76, 51.79, 35.99
α, β, γ (°)	90, 98.6, 90	90, 110.55, 90
Resolution (Å)	42–2.14 (2.22–2.14)*	30.7–1.66 (1.72–1.66)*
R_{sym} or R_{merge} (%)	6.1 (60)	3.7 (63.7)
$I/\sigma I$	12.5 (2.0)	8.1 (1.0)
Completeness (%)	91 (57)	94.2 (81.6)
Redundancy	2.8 (1.7)	2.5 (2.0)
Refinement		
Resolution (Å)	41.7–2.14	30.67–1.9
No. of reflections	7,572	7,556
R_{work}/R_{free}	19.5/23.2	19.2/23.9
No. of atoms	975	1,107
Protein	491	551
DNA	409	403
Water	75	137
Other ligands	—	16
B factors		
Protein	56	25
DNA	58	24
Water	56	30
Other ligands	—	47
rmsds		
Bond lengths (Å)	0.01	0.008
Bond angles (°)	1.06	1.009

*Refers to the highest-resolution shell.

Helices 2 and 3 form a helix–turn–helix motif, constituting an electropositive groove for the negatively charged DNA and acting as the primary interface with the LBS. The DNA exhibits virtually no bending distortion; however, there is slight widening of the major groove in order to accommodate the DNA recognition helix 3. Lys172 of helix 2 interacts with the sugar-phosphate backbone via van der Waal's interaction, helping to orient the DNA and to allow helix 3 to lie fully in the major groove. Residues from helix 3 account for the majority of the direct base readout and also contribute sugar-phosphate backbone interactions between the protein and DNA (Fig. 2 *C* and *D*). Interactions important for base readout include hydrogen-bonding interactions between Lys194 of the SHLQKY motif, O6 of guanine (G3), and N6 of adenine (A4), with nucleotides shown in bold and numbered (5′-T^1A^2**G^3A^4** $T^5A^6C^7G^8C^9A^{10}$-3′). These interactions are lost in the (5′-TA**TA**TTCGAA-3′) bound structure, with Lys194 adopting a different conformation and no longer involved in hydrogen-bonding interactions with the DNA, explaining the weaker binding of this DNA sequence (Table 1). Gln193 interacts with the complementary strand at position 5, hydrogen bonding with N6 of adenine in both DNA sequences. In addition, Arg185 interacts with the DNA backbone through its secondary amine and participates in a water-mediated hydrogen-bonding network with cytosine 7 in both structures. Arginine196 contacts the sugar-phosphate backbone, further stabilizing the protein–DNA complex (Fig. 2*D*). While no residues in helix 1 directly interact with the DNA, Arg146, part of the unstructured N-terminal extension, intercalates into the minor groove and interacts largely via van der Waal's forces and

PLANT BIOLOGY

Downloaded at Palestinian Territory, occupied on December 27, 2021
www.manaraa.com

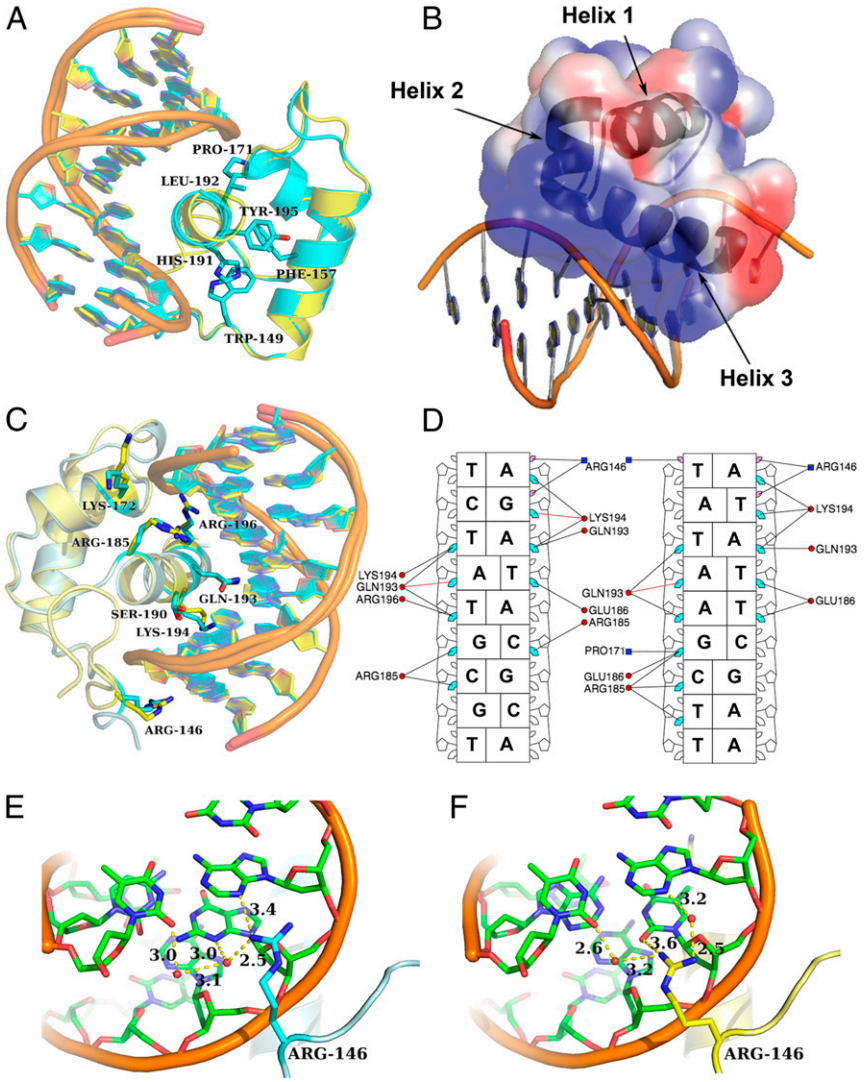

Fig. 2. Structure of LUX^{MYB} in complex with DNA. (*A*) Overlay of LUX^{MYB} structures in cyan (Protein Data Bank [PDB] ID code 5LXU) and yellow (PDB ID code 6QEC) with the hydrophobic core residues displayed as sticks and colored by atom with carbons in cyan (only 5LXU side chains are shown for clarity). The DNA sequences 5′-TAGATACGCA (cyan carbons) and 5′-TATATTCGAA (yellow carbons) are shown as sticks. (*B*) Electrostatic surface representation with electropositive to electronegative surfaces colored from blue to red and with helices indicated by arrows. (*C*) Overlay of LUX^{MYB}–DNA structures; amino acid residues interacting with the DNA are shown as sticks and colored by atom with carbons in cyan (5′-TAGATACGCA) or yellow (5′-TATATTCGAA). DNA is shown as a cartoon. (*D*) Simplified schematic from DNAproDB (49) of amino acids important for DNA binding and base readout with only direct base interactions shown for clarity. The LBS sequences are depicted without the first overhanging base, major groove interactions are shown in cyan, minor groove interactions are in purple, protein helices are in red circles, and loop residues are in blue squares. (*E* and *F*) Close-up view of Arg146 interactions with DNA colored by atom, with carbons in green. The proteins are colored as per *C*. Hydrogen-bonding interactions are shown as dotted lines, and distances are labeled. Water molecules are shown as red spheres. Arg146 adopts different conformations in the two structures.

a water-mediated hydrogen-bonding network with adenine 2 and guanine/thymine 3 of the bound DNA (5′-T**AG**ATACGCA-3′ and 5′-T**AT**ATTCGAA-3′) (Fig. 2 *E* and *F*). Interestingly, the Arg146 residue adopts different conformations in the two structures with different hydrogen-bonding networks, suggesting plasticity in Arg146–DNA interactions.

As Arg146 seems to act as a general "clamp" targeting the DNA minor groove, this residue was targeted for mutagenesis. The R146A mutation in both the LUX^{MYB} and LUX^{FL} was assayed for DNA binding by EMSAs. As predicted, the R146A mutation reduced the binding affinity for both LUX^{MYB} and LUX^{FL}, albeit with a greater effect depending on the DNA sequence (Table 1).

In Vivo Effects of LUX^{R146A}. We hypothesized that decreasing LUX DNA binding affinity would result in a less active EC and a phenotype intermediate between the wild type and the *lux-4* mutant, which lacks a functional DBD due to a premature stop codon. To test this, we transformed the *lux-4* mutant in the *Arabidopsis* Columbia-0 (Col-0) background with either *LUX* or *LUX^{R146A}* under the control of the native *LUX* promoter and examined hypocotyl length under short-day conditions at 22 °C and 27 °C and flowering time under long-day conditions at 22 °C. Transformation with the *pLUX:: LUX* construct resulted in complementation based on hypocotyl length (Fig. 3 *A–C* and *SI Appendix*, Fig. S4) and on flowering time, measured as the number of rosette leaves at time of bolting (Fig. 3 *D* and *E*). In contrast, *LUX^{R146A}* was not able to completely rescue the *lux-4* mutation, with hypocotyl length and flowering time intermediate between the wild type and *lux-4* (Fig. 3). Temperature-responsive growth was still observed in *LUX^{R146A}* but was more attenuated than in the

Downloaded at Palestinian Territory, occupied on December 27, 2021
www.manaraa.com

wild type or *lux-4* complemented with the wild-type gene (Fig. 3*C*). These data show that reduction in the binding affinity by the LUX^{R146A} mutation, as demonstrated in vitro, also had an in vivo effect.

Role of LUX, ELF3, and ELF4 in Complex Formation and DNA Binding. While LUX is required to bind DNA, complex formation is necessary for full EC activity (9, 16–18). The structural and mutagenesis experiments for LUX provided insight into DNA binding specificity and affinity but did not offer insight as to the roles of ELF3 or ELF4 in the EC. In order to understand the roles of these proteins, neither of which possesses a domain of known function, we reconstituted the EC and the LUX–ELF3 subcomplex in vitro and performed extensive EMSA experiments. As full-length ELF3 was not soluble, a urea refolding protocol was used followed by stepwise dialysis against decreasing urea concentrations to form the EC and LUX–ELF3 complexes. To confirm production of active complexes, EMSAs were performed using a 36-base pair (bp) fragment from the *PRR9* promoter containing a previously well-characterized LBS (10). As shown in Fig. 4 *A* and *B*, ELF3 and ELF4 alone did not interact with DNA as expected since neither protein is predicted to have a DBD. Addition of ELF4 to a solution containing LUX had no effect on LUX binding. However, titration of ELF3 with constant LUX and ELF4 concentrations resulted in the disappearance of the LUX–DNA band and the appearance of a higher-molecular weight band corresponding to the EC bound to DNA (Fig. 4*A* and *SI Appendix*, Fig. S5). Interestingly, without ELF4 present, LUX–ELF3 exhibited relatively poor DNA binding, with the appearance of a free DNA band that increases in intensity with increasing ELF3 concentration. No higher-molecular weight bands were observed with LUX–ELF3 alone (Fig. 4*C*). These results suggest that ELF4 is required for high-affinity DNA binding. To test this hypothesis, we titrated increasing concentrations of ELF4 with constant LUX and ELF3 concentrations. The free DNA band diminished in intensity, and the high-molecular weight band corresponding to the EC increased in intensity with increasing ELF4 concentrations, suggesting that ELF4 stabilizes the complex binding to DNA (Fig. 4*D*).

Effects of Temperature on EC Binding. As EC binding is affected by temperature in vivo, we used isothermal titration calorimetry (ITC) to determine whether LUX DNA binding activity is temperature dependent in vitro. The DNA binding constants of LUX^{FL} at 4 °C, 12 °C, and 27 °C were determined but demonstrated no strong temperature dependence, suggesting that ELF3 and ELF4 are needed to confer temperature sensitivity to EC–DNA binding (*SI Appendix*, Fig. S6).

Using our reconstituted EC, we tested this temperature dependence in vitro. Performing EMSAs with the same samples run in parallel at 4 °C, 15 °C, and 27 °C revealed highly attenuated binding by the complex with increased temperature (Fig. 5*A*). Only at the highest concentrations of the EC was a supershift visible for experiments performed at 15 °C, and this band was completely absent when performed at 27 °C, whereas samples at 4 °C exhibited strong binding as evidenced by a clear supershift corresponding to the EC–DNA complex.

To determine if ELF4 may stabilize the EC, allowing it to act at higher temperatures, we tested an ∼20-fold excess of ELF4 while keeping the concentrations of LUX and ELF3 the same as in the previous experiment. EMSAs were again performed at 4 °C, 15 °C, and 27 °C. A supershift was observed at the highest concentrations of ELF4 for all temperatures (Fig. 5*B*). This demonstrates that high concentrations of ELF4 stabilize EC binding, increasing affinity and allowing binding at higher temperatures, such as 27 °C.

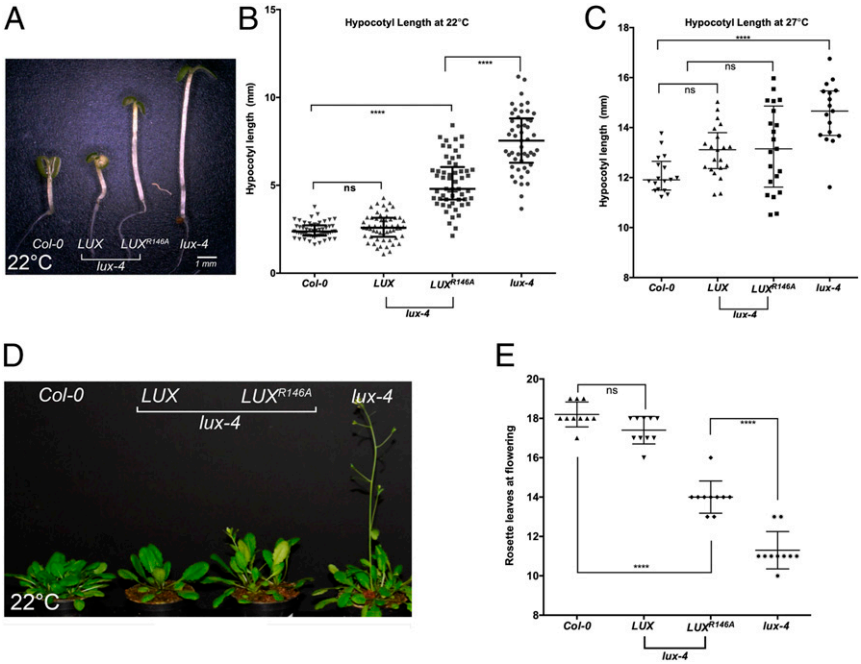

Fig. 3. Hypocotyl and flowering phenotypes for *Col-0*, *lux-4*, and *lux-4* expressing either LUX or LUX^{R146A}-transformed lines. (*A*) Representative hypocotyls from 7-d-old seedlings grown at 22 °C. (Scale bar, 1 mm.) (*B*) Hypocotyl length measurements from three independent lines pooled for seedlings grown at 22 °C. One-way ANOVA test was performed. The error bars represent the median value with interquartile ranges. ns, not significant. ****$P < 0.001$. (*C*) Hypocotyl length measurements from seedlings grown at 27 °C. ns, not significant. ****$P < 0.001$. (*D*) Representative images of plants grown at 22 °C on soil. (*E*) Number of rosette leaves at time of bolting from indicated genotypes. Error bars represent the mean with SD. All measurements were performed of plants from three independent lines for all transformed lines. ns, not significant. ****$P < 0.001$.

Downloaded at Palestinian Territory, occupied on December 27, 2021
www.manaraa.com

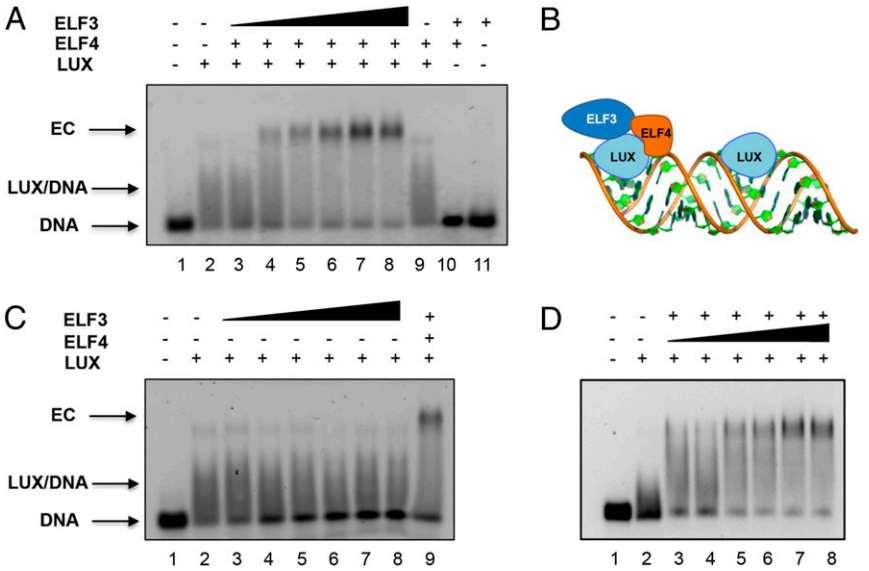

Fig. 4. EC and subcomplex interactions with DNA. (*A*) EMSAs of LUX–ELF3 and the EC in 2% agarose gels. DNA concentration was 30 nM. Reconstitution of the EC with LUX and ELF4 concentrations held constant at 200 and 1,000 nM, respectively, and increasing ELF3 concentrations (220 nM, 450 nM, 890 nM, 1.3 μM, 1.8 μM, and 2.2 μM). (*B*) Schematic of EC and LUX–DNA interactions. LUX is able to bind DNA independently of the EC; however, EC–DNA binding requires LUX. (*C*) LUX–ELF3 interactions with LUX concentration kept at 200 nM and ELF3 concentrations as per *A*. With increasing ELF3 concentration, the free DNA band increases in intensity, suggesting that LUX–ELF3 poorly binds DNA. (*D*) LUX and ELF3 concentrations held constant at 200 nM and ~1,000 nM, respectively, with increasing ELF4 concentrations (0, 250 nM, 500 nM, 1 μM, 2 μM, and 4 μM). ELF4 stabilizes EC binding.

Discussion

The EC not only plays an important role in the circadian clock but also, acts as a hub for integrating environmental cues and relaying this information directly to growth and developmental pathways through direct effects on target genes, including *GI*, *PRR7*, *PRR9*, and *PIF4* (26, 33, 34). Based on in vivo studies, the EC acts as a temperature-sensitive repressor of gene expression, with increased repression of target genes at lower temperatures. Whether temperature has a direct effect on EC binding to DNA, complex formation, or cofactor recruitment is not known. To address this deficit, we sought to provide a molecular in vitro model of LUX, ELF3, and ELF4 interactions in EC formation and to define the roles of the different proteins in DNA binding specificity and affinity in the context of complex formation.

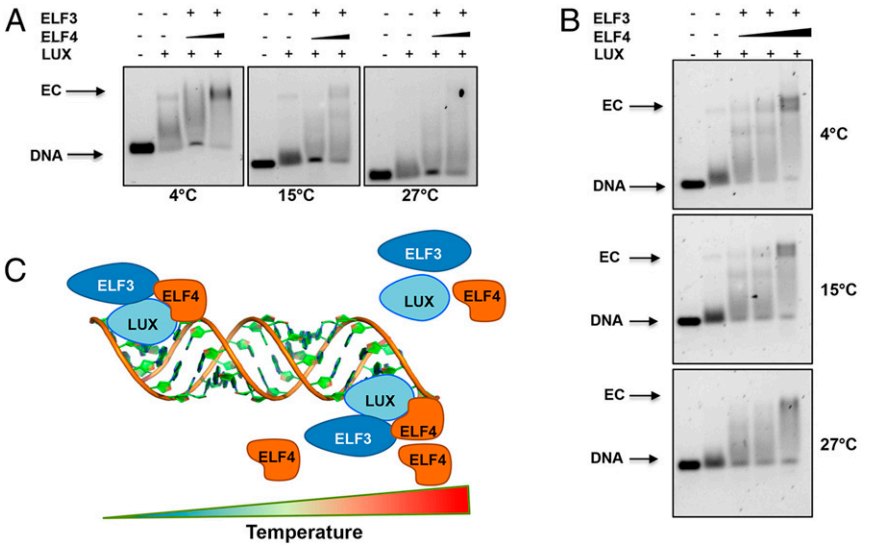

Fig. 5. Temperature dependency of EC binding and the effects of ELF4. (*A*) EC DNA binding assayed at 4 °C, 15 °C, and 27 °C. A band corresponding to the EC is visible at 4 °C and faintly visible at 15 °C, but it disappears at 27 °C using the same protein and DNA concentrations. EMSAs were run in parallel for 30 min at 90 V. Lanes are free DNA, DNA + LUX, DNA + LUX + ELF3 + ELF4 (~1:1:1), and DNA + LUX + ELF3 + ELF4 (~1:6:8) from left to right, respectively. DNA and LUX concentrations were 20 and 500 nM, respectively, for all lanes. (*B*) High concentrations of ELF4 restore EC binding to DNA at 27 °C. EMSAs were run in parallel for 30, 40, and 50 min for 27 °C, 15 °C, and 4 °C, respectively, to give approximately equal migration of the complexes. Lanes are free DNA, DNA + LUX, DNA + LUX + ELF3 + ELF4 (~1:1:1), DNA + LUX + ELF3 + ELF4 (~1:6:8), and DNA + LUX + ELF3 + ELF4 (~1:6:20) from left to right, respectively. DNA and LUX concentrations were as for *A*. (*C*) Schematic depiction of LUX, ELF3, and ELF4 interactions and DNA binding. The complex stably binds DNA at lower temperatures, while increasing temperatures result in complex dissociation from DNA. High ELF4 protein concentration is able to compensate and stabilize EC binding at higher temperatures.

Downloaded at Palestinian Territory, occupied on December 27, 2021
www.manaraa.com

Based on the in vitro and structural studies presented here, LUX provides the specificity and affinity necessary to target the entire EC to its cognate binding sites. The MYB domain is able to perform direct base readout of the core LBS. The plant-specific signature sequence, SH(A/L)QK(F/Y) of helix 3, provides the majority of direct interactions in the major groove of its cognate DNA. In addition, an N-terminal arginine Arg146, part of a flexible extension, is important for intercalation into the minor groove and acts as a DNA clamp. Arginine residues in flexible extensions are found in many other structurally diverse TFs, including homeodomain TFs and MADS (named for canonical members MCM1 from *Saccharomyces cerevisiae*, AGAMOUS from *Arabidopsis thaliana*, DEFICIENS from *Antirrhinum majus* and SRF from *Homo sapiens*) TF family members (35, 36). While these arginine residues are likely important for DNA shape readout by intercalating into the minor groove (37), they are often not required for direct base readout and may offer a general way to increase DNA binding affinity without a base specificity requirement. Mutating Arg146 of LUX to alanine decreased the DNA binding affinity of LUX while still retaining specificity based on both in vitro and in vivo assays. Based on in vitro K_d comparisons between LUX wild-type protein and the LUX^{R146A} mutant, we predicted weaker but not abolished EC activity in planta. Indeed, at 22 °C, an intermediate early flowering phenotype between the wild type and *lux-4* was observed for *lux-4* plants transformed with LUX^{R146A} under the control of the native *LUX* promotor.

While LUX is able to bind DNA alone both in vitro and in vivo, EC function requires the recruitment of the partner proteins, ELF3 and ELF4 (17, 38–40). In order to define the roles of ELF3 and ELF4 in DNA binding and EC function, different protein complexes were reconstituted in vitro. LUX and ELF3 have been shown to interact in yeast two-hybrid assays and in vivo (12). Here, we demonstrate that, in vitro, the LUX–ELF3 complex is a relatively poor binder of DNA, possibly due to the occlusion of the DBD by the largely unstructured ELF3 protein. ELF3 has been observed to impair DNA binding of PIF4 for the ELF3–PIF4 complex, acting to sequester the PIF4 transcription factor (41). This may be a general function of ELF3 in other TF complexes, although this intriguing hypothesis requires additional studies to confirm.

Based on our in vitro assays, ELF4 plays a key role in EC DNA binding activity, likely through tuning ELF3 structure via direct interactions. ELF3 and ELF4 interact based on yeast two-hybrid assays, whereas LUX does not interact directly with ELF4, as previously shown (12). ELF4, a small largely alpha helical protein, interacts with the middle region of ELF3, which also possesses a predicted alpha helical region (11). This interaction may be required in the EC to allow the DBD of LUX to access its cognate binding sites and stabilize complex binding to DNA. Titration series of increasing ELF4 concentrations demonstrate increased EC binding to DNA, highlighting the crucial role of ELF4 in the EC with respect to robust DNA binding of the complex. Indeed, previous modeling studies of the contributions to EC activity suggested that *ELF4* transcript levels are as powerful a predictor of EC target gene repression as using the full EC (*LUX*, *ELF3*, and *ELF4* transcript levels) and more predictive than *ELF3* alone (15). Thus, only with all three components, LUX, ELF3, and ELF4, do both DNA binding and target gene regulation occur, and ELF4 acts as a key modulator of this activity.

While LUX does not exhibit any temperature-sensitive DNA binding in vitro, the entire EC exhibits temperature-sensitive binding in planta. In order to reconcile these data, we performed EMSA experiments at 4 °C, 15 °C, and 27 °C. These data show that the EC binds more strongly at lower temperatures in vitro. At approximately equimolar LUX:ELF3:ELF4 concentrations, EC binding was observed at 4 °C and 15 °C but not at 27 °C. However, performing the same experiment using an ∼20-fold molar excess of ELF4 restored EC binding at 27 °C. These data suggest that ELF4 is able to modulate EC binding activity and to partially overcome the temperature dependence of EC binding when present in high concentrations, at least in vitro. These results suggest that ELF4 expression levels may play an important role in planta with respect to EC function and remain to be investigated in a physiological context.

The EC plays dual roles as a core clock component and as an integrator of temperature data into plant developmental pathways. Here, we provide important structural and biochemical data outlining the different functions of the three proteins in DNA binding specificity and affinity at different temperatures. The full EC displays temperature-sensitive DNA binding with ELF4 concentration able to stabilize EC binding even at higher temperatures. Thus, ELF4 protein levels are critical in the repression of EC target genes, increasing the DNA binding activity of the EC. Intriguingly, this suggests that modulating ELF4 expression may provide a generally applicable way to alter plant thermoresponsiveness in plants within the ambient temperature range.

Materials and Methods

Protein Binding Microarrays. LUX (LUX FL; The Arabidopsis Information Resource [TAIR] At3g46640.1) and LUX^{MYB} (amino acid residues 139 to 200) were cloned into the pETM41 vector to obtain MBP translational protein fusions. The recombinant proteins were expressed in *Escherichia coli* BL21 cells, and DNA binding specificities were determined using PBMs (PBM11) as previously described (30, 31).

Construct Design and Protein Expression. Point mutations LUX^{R146A} and LUX^{P171L} were produced via Quikchange (Agilent) according to the manufacturer's protocol. *LUX*, LUX^{MYB}, LUX^{R146A}, and *ELF4* (TAIR At2g40080.1) were cloned into the expression vector pESPRIT002 using standard protocols (42, 43), with all constructs containing a TEV protease-cleavable N-terminal 6xHis tag. Recombinant proteins were expressed in *E. coli* Rosetta2 (DE3) pLysS (LUX) or BL21 Codon Plus RIL cells (ELF4). *LUX* and LUX^{P171L} were cloned into the pTnT vector and expressed using the Promega SP6 High Yield Expression System for EMSAs shown in *SI Appendix*, Fig. S3. Selenomethionine (SeMet)-derived LUX^{MYB} protein was produced in M9 minimal medium using the nonauxotrophic *E. coli* strain Rosetta2 (DE3) pLysS cells according to standard protocols (44). Full-length *ELF3* (TAIR At2g25930.1) was cloned into the pACEBac1 (45) vector and produced in *Sf*21 insect cells (Invitrogen) using the baculovirus expression system.

Protein Purification. LUX^{FL}, LUX^{MYB}, and SeMet LUX^{MYB} proteins were isolated following the same purification protocol. Harvested cells were resuspended in 200 mM *N*-cyclohexyl-3-aminopropanesulfonic acid (CAPS), pH 10.5, 500 mM NaCl, 1 mM Tris(2-carboxyethyl)phosphine (TCEP), and protease inhibitors (Roche), and then, they were sonicated and centrifuged. The soluble proteins were purified by Ni-affinity chromatography. The N-terminal 6xHis tag was cleaved with TEV protease, and the protein was further purified using a heparin (LUX^{MYB}) or Superdex 200 (LUX^{FL}) column (GE Healthcare) into a final buffer of 50 mM CAPS, pH 9.7, 100 mM NaCl, and 1 mM TCEP.

For ELF4 protein, harvested cells were resuspended in 20 mM Tris, pH 8.0, 500 mM NaCl, 1 mM TCEP, and protease inhibitors. Purification was as per LUX^{FL}, with final buffer of 20 mM Tris, pH 8.0, 100 mM NaCl, and 1 mM TCEP.

For ELF3, harvested cells were resuspended in 8 M urea, 1 mM TCEP, sonicated and centrifuged. The soluble protein was purified by Ni-affinity chromatography under denaturing conditions.

Protein Crystallization and Data Collection. Single-strand DNA oligomers were annealed and mixed with LUX^{MYB} at a 1.2:1 ratio, and then, they were used without further purification. Protein–DNA complexes were crystallized using the hanging drop method as previously described (46).

Diffraction data were collected at 100 Kelvin (K) at the European Synchrotron Radiation Facility, Grenoble, France. Data collection and refinement statistics are given in Table 2. The structures are deposited under Protein Data Bank ID codes 5LXU and 6QEC.

EMSAs. A 36-bp DNA oligonucleotide (5′-ATG ATG TCT TCT CAA GAT TCG ATA AAA ATG GTG TTG-3′) from the *PRR9* promoter containing a LUX DNA

Downloaded at Palestinian Territory, occupied on December 27, 2021

www.manaraa.com

Table 3. For EMSAs, a 36-bp DNA oligonucleotide using a backbone from the *PRR9* promoter was generated with variations of the LBS (underlined)

DNA oligo	DNA sequence
Oligo 1	5′-ATGATGTCTTCTCA**AGATTCGA**TAAAAATGGTGTTG-3′
Oligo 2	5′-ATGATGTCTTCTCA**AGATACGC**TAAAAATGGTGTTG-3′
Oligo 3	5′-ATGATGTCTTCTC**AAGATCTT**ATAAAAATGGTGTTG-3′
Oligo 4	5′-ATGATGTCTTCT**CGGATCCG**ATAAAAATGGTGTTG-3′
Oligo 5	5′-ATGATGTCTTCTCG**AATATTCG**ATAAAAATGGTGTTG-3′

LUX DNA binding sites are bold and underlined.

binding site (bold and underlined in Table 3) was used for EMSAs, and the core LBS was mutated to yield different sequences (Table 3).

DNA was Cy5 labeled for visualization and used at a final concentration of 10 nM for polyacrylamide gel electrophoresis (PAGE) and 20 to 30 nM for agarose gels. Protein and DNA were incubated at room temperature in binding buffer (10 mM Tris, pH 7.0, 50 mM NaCl, 1 mM $MgCl_2$, 1 mM TCEP, 3% glycerol, 28 ng/μL herring sperm DNA, 20 μg/mL bovine serum albumin (BSA), 2.5% 3-cholamidopropyl dimethylammonio 1-propanesulfonate (CHAPS), 1.25 mM spermidine), and protein–DNA complexes were run on a 8% polyacrylamide gel or a 2% agarose gel using 0.5× tris-borate-EDTA (TBE) buffer in nondenaturing conditions at 4 °C.

Protein concentration was varied from 0 to 1,000 nM for LUX^{MYB} and LUX^{FL} experiments. For LUX–ELF3 and LUX–ELF3–ELF4 experiments, all tested complexes were reconstituted by mixing the proteins of interest in 6 M urea followed by a 1-M incremental stepwise dialysis to 0 M urea into a final buffer of 50 mM sodium phosphate, pH 7.6, 100 mM NaCl, and 1 mM TCEP. For ELF3 titrations, LUX and ELF4 concentrations were constant at 200 nM and 0 or 1 μM, respectively, while the ELF3 concentration was varied from 220 nM to 2.2 μM (220 nM, 450 nM, 890 nM, 1.3 μM, 1.8 μM, 2.2 μM). For ELF4 titrations, LUX and ELF3 concentrations were constant, with ELF4 concentration varied from 0 nM to 4 μM (0, 250 nM, 500 nM, 1 μM, 2 μM, 4 μM). Proteins and DNA were incubated in binding buffer (10 mM Tris, pH 7.0, 1 mM $MgCl_2$, 1 mM TCEP, 6% glycerol, 28 ng/μL herring sperm DNA, 20 μg/mL BSA, 2.5% CHAPS, 1.25 mM spermidine) at room temperature, and protein–DNA complexes were run on a 2% agarose gel using 0.5× TBE buffer in nondenaturing conditions at 4 °C, except for temperature dependency experiments. For temperature dependence, all experiments and gels were run at the indicated temperatures using the same starting binding reactions.

ITC Measurements for LUX^{FL}–*PRR9* DNA. ITC titration experiments were performed on a Microcal iTC200 instrument in 20 mM Tris, pH 7.0, 50 mM NaCl, and 1 mM $MgCl_2$ buffer. *PRR9* promoter LBS 10-mer DNA (5′-AAGATTCGAT-3′, 300 μM) was titrated into 20 μM LUX^{FL} at 4 °C, 12 °C, and 27 °C. LUX^{FL} concentration was determined from absorbance at 280 nm. Data were processed with Origin to extract the thermodynamic parameter K_d ($1/K_a$). All titrations fit the single-binding site mechanism.

Plasmid Construction and Generation of Transgenic Plants. For the *lux-4* p*LUX*::LUX^{R146A}, *lux-4 pLUX::LUX* constructs, an ∼800-bp upstream fragment of *LUX* was PCR amplified from genomic DNA. Full-length coding sequence (CDS) of *LUX* and LUX^{R146A} was PCR amplified from the pESPRIT002 expression vector containing the respective CDS with an N-terminal FLAG tag (DYKDDDDK) added (*SI Appendix*, Fig. S7). NEBuilder HiFi DNA Assembly Kit (E2621S; NEB) was used for assembly with the vector backbone (pFP101 containing the *At2S3* promoter-driven GFP for selection of transformants) (47). A list of primers is in *SI Appendix*, Table S1. Transgenic plants were generated using the floral dip method (48).

Plant Material and Cultivation Conditions. For hypocotyl measurements, material was collected from 7-d-old seedlings grown in FitoClima D1200 (Aralab) growth chambers at 22 °C (short day [SD], 8-h light/16-h dark). Hypocotyl measurements were performed on the second generation progeny (T2) of plants with 15 to 25 plants for three independent lines. For flowering phenotype analysis, primary transformants were selected for the transgene, sown on soil, and transferred to long day (LD) conditions after stratification (4 °C, 3 d). Flowering time was determined in randomly distributed plants according to number of rosette leaves at the time of bolting (10 plants for the wild type, *lux-4*, *lux-4 pLUX::LUX*^{R146A}, and *lux-4 pLUX::LUX*).

Data Availability Statement. All crystallographic data are deposited in the Protein Data Bank. All other data discussed in the paper will be made available to readers on request.

ACKNOWLEDGMENTS. We thank Francois Parcy for helpful discussions, Elodie Pierre and Caroline Mas for technical assistance, the European Synchrotron Radiation Facility beamline staff on ID29 and ID23-2, and Darren Hart and Philippe Mas for the ESPRIT002 vector. This work used the platforms of the Grenoble Instruct-European Research Infrastructure Consortium Center within the Grenoble Partnership for Structural Biology, supported by the French Infrastructure for Integrated Structural Biology (Agence National de la Recherche grant ANR-10-INBS-05-02) and the Grenoble Alliance for Integrated Structural and Cell Biology (grant ANR-10-LABX-49-01). Access to the European Molecular Biology Laboratory High-Throughput Crystallisation Laboratory (EMBL-HTX) was provided by the European Community's Seventh Framework Program (FP7) under grant agreement 283570. Additional platform support was financed within the Chemistry-Biology-Health (CBH), University Grenoble Alpes graduate school (Ecoles Universitaires de Recherche) CBH-EUR-GS (grant ANR-17-EURE-0003). This work was supported by the French National Research Agency programs Tempsens (grant ANR-19-CE20-0021-01 to C.Z.), the Commissariat à l'Énergie Atomique et aux Énergies Alternatives thesis student program and Raman Charpak Fellowship (to A.N.) and a Spanish Ministry of Science and Innovation (grant BIO2017-86651-P to J.M.F.-Z.).

1. A. N. Dodd *et al.*, Plant circadian clocks increase photosynthesis, growth, survival, and competitive advantage. *Science* **309**, 630–633 (2005).
2. C. R. McClung, Plant circadian rhythms. *Plant Cell* **18**, 792–803 (2006).
3. S. L. Harmer, The circadian system in higher plants. *Annu. Rev. Plant Biol.* **60**, 357–377 (2009).
4. P. A. Salomé, Q. Xie, C. R. McClung, Circadian timekeeping during early Arabidopsis development. *Plant Physiol.* **147**, 1110–1125 (2008).
5. C. R. McClung, The genetics of plant clocks. *Adv. Genet.* **74**, 105–139 (2011).
6. D. H. Nagel, S. A. Kay, Complexity in the wiring and regulation of plant circadian networks. *Curr. Biol.* **22**, R648–R657 (2012).
7. Z. J. Chen, Genomic and epigenetic insights into the molecular bases of heterosis. *Nat. Rev. Genet.* **14**, 471–482 (2013).
8. K. A. Hicks, T. M. Albertson, D. R. Wagner, EARLY FLOWERING3 encodes a novel protein that regulates circadian clock function and flowering in Arabidopsis. *Plant Cell* **13**, 1281–1292 (2001).
9. S. P. Hazen *et al.*, LUX ARRHYTHMO encodes a Myb domain protein essential for circadian rhythms. *Proc. Natl. Acad. Sci. U.S.A.* **102**, 10387–10392 (2005).
10. A. Helfer *et al.*, LUX ARRHYTHMO encodes a nighttime repressor of circadian gene expression in the Arabidopsis core clock. *Curr. Biol.* **21**, 126–133 (2011).
11. E. Herrero *et al.*, EARLY FLOWERING4 recruitment of EARLY FLOWERING3 in the nucleus sustains the Arabidopsis circadian clock. *Plant Cell* **24**, 428–443 (2012).
12. D. A. Nusinow *et al.*, The ELF4-ELF3-LUX complex links the circadian clock to diurnal control of hypocotyl growth. *Nature* **475**, 398–402 (2011).
13. B. Y. Chow, A. Helfer, D. A. Nusinow, S. A. Kay, ELF3 recruitment to the PRR9 promoter requires other Evening Complex members in the Arabidopsis circadian clock. *Plant Signal. Behav.* **7**, 170–173 (2012).
14. T. Mizuno *et al.*, Ambient temperature signal feeds into the circadian clock transcriptional circuitry through the EC night-time repressor in Arabidopsis thaliana. *Plant Cell Physiol.* **55**, 958–976 (2014).
15. D. Ezer *et al.*, The evening complex coordinates environmental and endogenous signals in Arabidopsis. *Nat. Plants* **3**, 17087 (2017).
16. K. Onai, M. Ishiura, PHYTOCLOCK 1 encoding a novel GARP protein essential for the Arabidopsis circadian clock. *Genes Cells* **10**, 963–972 (2005).
17. M. R. Doyle *et al.*, The ELF4 gene controls circadian rhythms and flowering time in Arabidopsis thaliana. *Nature* **419**, 74–77 (2002).
18. K. A. Hicks *et al.*, Conditional circadian dysfunction of the Arabidopsis early-flowering 3 mutant. *Science* **274**, 790–792 (1996).
19. K. Nozue *et al.*, Rhythmic growth explained by coincidence between internal and external cues. *Nature* **448**, 358–361 (2007).
20. M. S. Box *et al.*, ELF3 controls thermoresponsive growth in Arabidopsis. *Curr. Biol.* **25**, 194–199 (2015).
21. P. Gawroński *et al.*, A distorted circadian clock causes early flowering and temperature-dependent variation in spike development in the Eps-3Am mutant of einkorn wheat. *Genetics* **196**, 1253–1261 (2014).
22. S. F. Undurraga *et al.*, Background-dependent effects of polyglutamine variation in the Arabidopsis thaliana gene ELF3. *Proc. Natl. Acad. Sci. U.S.A.* **109**, 19363–19367 (2012).
23. A. Raschke *et al.*, Natural variants of ELF3 affect thermomorphogenesis by transcriptionally modulating PIF4-dependent auxin response genes. *BMC Plant Biol.* **15**, 197 (2015).
24. A. Castillon, H. Shen, E. Huq, Phytochrome interacting factors: Central players in phytochrome-mediated light signaling networks. *Trends Plant Sci.* **12**, 514–521 (2007).
25. P. Leivar, P. H. Quail, PIFs: Pivotal components in a cellular signaling hub. *Trends Plant Sci.* **16**, 19–28 (2011).
26. S. V. Kumar *et al.*, Transcription factor PIF4 controls the thermosensory activation of flowering. *Nature* **484**, 242–245 (2012).

Downloaded at Palestinian Territory, occupied on December 27, 2021
www.manaraa.com

27. D. Lucyshyn, P. A. Wigge, Plant development: PIF4 integrates diverse environmental signals. *Curr. Biol.* **19**, R265–R266 (2009).
28. P. Hornitschek, S. Lorrain, V. Zoete, O. Michielin, C. Fankhauser, Inhibition of the shade avoidance response by formation of non-DNA binding bHLH heterodimers. *EMBO J.* **28**, 3893–3902 (2009).
29. H. Huang, D. A. Nusinow, Into the evening: Complex interactions in the Arabidopsis circadian clock. *Trends Genet.* **32**, 674–686 (2016).
30. J. M. Franco-Zorrilla *et al*., DNA-binding specificities of plant transcription factors and their potential to define target genes. *Proc. Natl. Acad. Sci. U.S.A.* **111**, 2367–2372 (2014).
31. M. Godoy *et al*., Improved protein-binding microarrays for the identification of DNA-binding specificities of transcription factors. *Plant J.* **66**, 700–711 (2011).
32. C. Kanei-Ishii *et al*., The tryptophan cluster: A hypothetical structure of the DNA-binding domain of the myb protooncogene product. *J. Biol. Chem.* **265**, 19990–19995 (1990).
33. M. A. Koini *et al*., High temperature-mediated adaptations in plant architecture require the bHLH transcription factor PIF4. *Curr. Biol.* **19**, 408–413 (2009).
34. S. N. Gangappa, S. Berriri, S. V. Kumar, PIF4 coordinates thermosensory growth and immunity in Arabidopsis. *Curr. Biol.* **27**, 243–249 (2017).
35. T. R. Bürglin, M. Affolter, Homeodomain proteins: An update. *Chromosoma* **125**, 497–521 (2016).
36. S. Kappel, R. Melzer, F. Rumpler, C. Gafert, G. Theissen, The floral homeotic protein SEPALLATA3 recognizes target DNA sequences by shape readout involving a conserved arginine residue in the MADS-domain. *Plant J.* **95**, 341–357 (2018).
37. A. Mathelier *et al*., DNA shape features improve transcription factor binding site predictions in vivo. *Cell Syst.* **3**, 278–286.e4 (2016).
38. S. P. Hazen *et al*., Rapid array mapping of circadian clock and developmental mutations in Arabidopsis. *Plant Physiol.* **138**, 990–997 (2005).
39. M. T. Zagotta, S. Shannon, C. Jacobs, D. R. Meeks-Wagner, Early-flowering mutants of A. thaliana. *Aust. J. Plant Physiol.* **19**, 411–418 (1992).
40. M. T. Zagotta *et al*., The Arabidopsis ELF3 gene regulates vegetative photomorphogenesis and the photoperiodic induction of flowering. *Plant J.* **10**, 691–702 (1996).
41. C. Nieto, V. López-Salmerón, J. M. Davière, S. Prat, ELF3-PIF4 interaction regulates plant growth independently of the Evening Complex. *Curr. Biol.* **25**, 187–193 (2015).
42. D. J. Hart, F. Tarendeau, Combinatorial library approaches for improving soluble protein expression in Escherichia coli. *Acta Crystallogr. D Biol. Crystallogr.* **62**, 19–26 (2006).
43. D. Guilligay *et al*., The structural basis for cap binding by influenza virus polymerase subunit PB2. *Nat. Struct. Mol. Biol.* **15**, 500–506 (2008).
44. S. Doublié, Production of selenomethionyl proteins in prokaryotic and eukaryotic expression systems. *Methods Mol. Biol.* **363**, 91–108 (2007).
45. L. S. Vijayachandran *et al*., Robots, pipelines, polyproteins: Enabling multiprotein expression in prokaryotic and eukaryotic cells. *J. Struct. Biol.* **175**, 198–208 (2011).
46. C. S. Silva, X. Lai, M. Nanao, C. Zubieta, The Myb domain of LUX ARRHYTHMO in complex with DNA: Expression, purification and crystallization. *Acta Crystallogr. F Struct. Biol. Commun.* **72**, 356–361 (2016).
47. S. Bensmihen *et al*., Analysis of an activated ABI5 allele using a new selection method for transgenic Arabidopsis seeds. *FEBS Lett.* **561**, 127–131 (2004).
48. R. T. Fraley *et al*., The SEV system: A new disarmed Ti plasmid vector system for plant transformation. *Nat. Biotechnol.* **3**, 629–635 (1985).
49. J. M. Sagendorf, H. M. Berman, R. Rohs, DNAproDB: An interactive tool for structural analysis of DNA-protein complexes. *Nucleic Acids Res.* **45**, W89–W97 (2017).

Downloaded at Palestinian Territory, occupied on December 27, 2021

www.manaraa.com